Multivariable classical Prandtl-Ishlinskii hysteresis modeling and compensation and sensorless control of a nonlinear 2-dof piezoactuator

Micky RAKOTONDRABE

Abstract: A multivariable approach of modeling and feedforward control of rate-independent hysteresis in multi-DOF piezoelectric actuators is proposed in this paper. For that, the classical Prandtl-Ishlinskii (CPI) hysteresis model is extended into multivariable. Then, based on the inverse multiplicative structure and on the multivariable CPI model, a compensator is suggested. The proposed compensator does not require an extra-calculation: as soon as the model is identified, the compensator is obtained by structure. Furthermore, inversion of the model is avoided. Additionally to the hysteresis suppression, the multivariable compensator permits to reduce the cross-couplings between the axes which is not possible with standard techniques. The modeling and the free-inversion compensator are afterwards applied to a two-degrees of freedom (2-dof) piezoactuator. The extensive investigated experimental tests demonstrate that the strong cross-couplings and the strong hysteresis in the two axes can be substantially reduced and linearized respectively.

Keywords: Multivariable hysteresis, classical Prandtl-Ishlinskii, rate-independent hysteresis nonlinearity, nonlinearity compensation, free-inversion, inverse multiplicative structure, nonlinear piezoelectric actuators, smart materials, multiple degrees of freedom.

1. INTRODUCTION

Smart materials (piezoelectric ceramics, magnetostrictive, etc.) are widely used in the development of actuators devoted to precise positioning applications. These applications include microassembly, micromanipulation, microrobotics, in-body exploratory robots, micro-hydraulic valve control, surface scanning and characterization with microscopy, bio-manipulation [1–5]. Unfortunately, hysteresis nonlinearity is a phenomenon found in these smart materials which makes the actuators lose their final accuracy. In view of this loss of accuracy, open-loop (or feedforward) control approach of the hysteresis has been widely investigated (Fig. 1). The problem consists in modeling the hysteretic process of input $u(t)$ and of output $y(t)$ with a hysteresis operator $y(t) = \Gamma(u(t),t)$ and then finding a compensator $\Gamma^c(y_r(t),t)$ such that $y(t) = y_r(t)$ for $t > t_1$ (with $t_1 \geq 0$), $y_r(t)$ being the reference. However, the hysteresis model $\Gamma(u(t),t)$ is a strong nonlinear operator which raises a challenge in the finding of the related compensator $\Gamma^c(y_r(t),t)$. To reduce this difficulty, it is often admitted in piezoelectric actuators that the model $\Gamma(u(t),t)$ can be separated into a rate-independent hysteresis operator $\Gamma(u(t))$ cascaded with a linear dynamics [2,6,7]. Such architecture is called Hammerstein architecture. With this simplification, the compensator to be calculated is a rate-independent compensator $\Gamma^c(y_r(t))$. Relative to feedback control, feedforward control presents the major advantage that no sensor is required and therefore a high level of packageability is obtained. This is essential in most of the above mentionned applications where there is a great lack of sensors to make the feedback. In fact, either they are bulky, not embeddable, expensive and not adapted to measure the actuators signals; or they are embeddable but do not have the required performances (resolution, accuracy and bandwidth of measurement) [6]. In return, feedforward control is sensitive to model uncertainties and this is why it is important to have a precise model $\Gamma(u(t))$ before the calculation of the compensator.

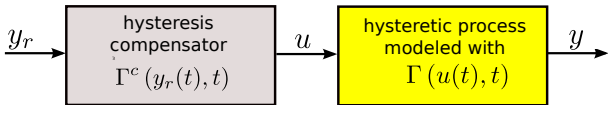

Fig 1: Schematic diagram of the feedforward control of a hysteretic process.

The literature is abundant regarding the modeling of hysteresis in smart materials. Different approaches have been raised to formulate $\Gamma(u(t))$. However, only some of the investigated approaches address both the modeling and the compensation. These hysteresis modeling and

Automatic Control and Micro-Mechatronic Systems (AS2M) Department FEMTO-ST Institute
UBFC / Univ Franche-Comté / CNRS
24 rue Alain Savary, Besançon 25000, France.
Corresponding author: mrakoton@femto-st.fr

compensation investigations include: the Bouc-Wen approach [8,9], the polynomial [10], the lookup tables [11], the Preisach [7,12–16], the Phase-Preisach combined approach [17], the Prandtl-Ishlinskii approaches [6,18–25], and other techniques [26,27].

All the above cited endeavors dealt with monovariable hysteresis which can only be used when the actuators and the systems have one degree of freedom (dof), i.e. they are single-input-single-output (SISO). Nonetheless, the raise of actuators and systems with multiple dof [3,28,29] gives the necessity to develop multivariable hysteresis models and compensators, i.e. multi-input-multi-output (MIMO). The additional challenge posed in such multi-dof systems is the presence of strong cross-couplings. Apart from the hysteresis, these cross-couplings favor the loss of accuracy in the final performances.

The first formulation of multivariable hysteresis model is the so-called vector Preisach hysteresis developed by Mayergoyz [30]. The principle consists in extending a Preisach model into bi-variable hysteresis. In fact, the vector hysteresis is based on the projection of a scalar hysteresis $\Gamma(u(t))$ along two directions x and y to yield vector components with a constraint parameter $\phi(t)$: $\Gamma_x(u(t)) = \Gamma(u(t))\,cos(\phi(t))$ and $\Gamma_y(u(t)) = \Gamma(u(t))\,sin(\phi(t))$. Further, the concept of vector hysteresis initially developed for a Preisach approach has been transposed to the play/stop-operators based hysteresis approach [31, 32]. Because of the circular constraint with the parameter $\phi(t)$, vector models are well adapted to formulate the hysteresis in rotative magnetic systems with, for instance, the magnetic field as input $u(t)$ and the vector magnetization as output [33, 34]. They cannot however track the hysteresis in multiple degrees of freedom where the cross-couplings are completely independent. Moreover, the number of inputs and of that of the outputs are limited to two respectively. Recently, the Bouc-Wen modeling and compensation have been extended into multivariable to surpass these limitations [9] which presented several advantages. First there is no restriction in the independency of the cross-couplings. Second, the number of the inputs is generalized (p-inputs) as well as the number of outputs (m-outputs). Finally, the system can be rectangular (p-inputs and m-inputs) or square (p-inputs and p-outputs). Another main advantage of the Bouc-Wen techniques is the simplicity and compactness of the expressions, permitting a structural analysis or synthesis [8]. However, due to the low number of parameters in these techniques, the class of hysteresis that they can model very precisely is limited.

An interesting hysteresis modeling technique that permits a high precision and real-time implementation possibility is the classical Prandtl-Ishlinskii technique. The principle is that a complex hysteresis curve is approximated by the superposition of many elementary hysteresis (called hysterons) $\gamma(u(t))$. Increasing the number of the hysterons ameliorates the precision of the model. The hysteron itself is a play-operator (or backlash operator) which is well convenient for real-time implementation. So far, the classical Prandtl-Ishlinskii technique has been used to model and to control piezoelectric actuators efficiently. To derive the compensator or feedforward controller $\Gamma^c(y_r(t))$, an inverse, an approximate inverse or an equivalent of the inverse of the classical Prandtl-Ishlinskii model $\Gamma(y_r(t))$ is calculated. There are different ways to synthesize the compensator. In [22], we proposed a compensator $\Gamma^c(y_r(t))$ as a restructuration of the initial model $\Gamma(y_r(t))$ by using the inverse multiplicative scheme. The advantages of the new compensator are double. First we avoid the direct inversion of the model which necessitated the invertibility conditions and which therefore limited the modeling applications. Second, we avoid extra-calculation of the compensator parameters because as soon as the initial model is identified, the compensator is derived by restructuration. These Prandtl-Ishlinskii modeling and compensation techniques are only usable on systems with one dof (SISO case), which restricts their utilization to hysteresis without cross-couplings.

1.1. Novelty of the paper

The contributions of this paper are:

- the extension of the classical Prandtl-Ishlinskii model into a multivariable classical Prandtl-Ishlinskii model capable to approximate hysteresis in systems with multiple dof. The novel multivariable model is given for the general case of rectangular systems (m inputs and p outputs) along with an identification procedure is also proposed.

- a new multivariable compensator (feedforward controller) for the multivariable classical Prandtl-Ishlinskii model. The compensator is limited for square systems only: m inputs and m outputs,

- and an illustrative example with a 2-dof piezoelectric actuator (piezoactuator) accompanied by extensive experiments and discussions. Comparison of the performances from the new multivariable compensator with those of the existing technique is particularly studied and analyzed.

1.2. Organization of the paper

The remainder of this paper is organized as follows. First, we give the preliminaries on the classical Prandtl-Ishlinskii modeling and identification in Section. 2. which is valid for moniovariable (SISO) case. Then, we detail in Section. 3. the proposed multivariable classical Prandtl-Ishlinskii model (MIMO case) and its identification procedure. The new multivariable compensator is afterwards presented in Section. 4.. Section. 5. presents the application of the suggested modeling, identification and compensation approach to a 2-dof piezoactuator. Comparison with existing technique is carried out and discussed in the same section. Finally, we give in Section. 6. and Section. 7. some discussion and the conclusions respectively.

2. PRELIMINARIES ON THE CLASSICAL PRANDTL-ISHLINSKII TECHNIQUE

The classical Prandtl-Ishlinskii model is a class of hysteresis models in which the model is a superposition of several elementary operators called hysterons. In the classical Prandtl-Ishlinskii model, the hysteron is the backlash (or play) operator. The backlash itself, denoted $\gamma(u(t))$ (that we alternately denote γ or $\gamma(u)$), of input $u(t)$ and of output $y(t)$, is an operator defined by the following equations:

$$\begin{cases} y(t) = \gamma(u) = \max\{u(t) - r, \min\{u(t) + r, y(t-T)\}\} \\ y(0) = y_0 \end{cases} \tag{1}$$

where r is the threshold and T is the refresh time.

The classical Prandtl-Ishlinskii hysteresis model $\Gamma(u(t))$, that we alternately denote Γ or $\Gamma(u)$, is therefore the superposition of several backlashes γ_i each one having a threshold r_i and being weighted by w_i [35]:

$$\begin{cases} y(t) = \Gamma(u) = \sum_{i=1}^{n} w_i \cdot \gamma_i(u) \\ = \sum_{i=1}^{n} w_i \cdot \max\{u(t) - r_i, \min\{u(t) + r_i, y_{ei}(t-T)\}\} \\ \\ y(0) = y_0 \end{cases} \tag{2}$$

where n is the number of hysterons and y_{ei} is the i^{th} elementary output (output of the i^{th} backlash).

The parameters to be identified are r_i and w_i. They can be identified through a least-square optimization [18], or using the closed-form presented in [22] that we remind in the Appendix.

The classical Prandtl-Ishlinskii model is capable of modeling the hysteresis only in systems having one degree of freedom. In the next section, we present its extension into multivariable classical Prandtl-Ishlinskii model.

3. A MULTIVARIABLE CLASSICAL PRANDTL-ISHLINSKII MODEL AND ITS IDENTIFICATION PROCEDURE

In this section, we present a novel multivariable classical Prandtl-Ishlinskii model capable of accounting for the hysteresis nonlinearity and the hysteresis cross-couplings in systems having several degrees of freedom. Its identification procedure is also detailed. The general case of a rectangular system is considered: m inputs and p outputs.

3.1. General definitions and properties

First we provide some definitions related to multivariable hysteresis.

Definition 3..1: A multivariable rate-independent hysteresis $\Gamma(U(t))$ is a vector of operators that have an input $U(t) = \begin{pmatrix} u_1(t) & u_2(t) & \cdots & u_m(t) \end{pmatrix}^T$ and an output $Y(t) = \begin{pmatrix} y_1(t) & y_2(t) & \cdots & y_p(t) \end{pmatrix}^T$ such that

$$Y(t) = \Gamma(U(t)) \Leftrightarrow \begin{pmatrix} y_1(t) \\ y_2(t) \\ \vdots \\ y_p(t) \end{pmatrix} = \begin{pmatrix} \Gamma_1(u_1(t), u_2(t), \cdots, u_m(t)) \\ \Gamma_2(u_1(t), u_2(t), \cdots, u_m(t)) \\ \vdots \\ \Gamma_p(u_1(t), u_2(t), \cdots, u_m(t)) \end{pmatrix}$$

Similarly to the multivariable classical Bouc-Wen model [9], let us assume that the hysteresis are additive. Consequently, the multivariable nonlinear model in Def. 3..1 becomes:

$$Y(t) = \begin{pmatrix} y_1(t) \\ y_2(t) \\ \vdots \\ y_p(t) \end{pmatrix} = \Gamma(U(t)) = \begin{pmatrix} \sum_{k=1}^{m} \Gamma_{1k}(u_k(t)) \\ \sum_{k=1}^{m} \Gamma_{2k}(u_k(t)) \\ \vdots \\ \sum_{k=1}^{m} \Gamma_{pk}(u_k(t)) \end{pmatrix} \tag{3}$$

where each element $\Gamma_{lk}(u_k(t))$ ($l = 1 \cdots p$ and $k = 1 \cdots m$) is either a hysteresis nonlinearity or a linear gain, but at least one of them is a hysteresis. With this condition, the operator $\Gamma(U(t))$ is therefore called multivariable hysteresis. In many systems using piezoelectric or magnetic actuators, all or almost all the diagonal Γ_{ll} elements are hysteresis [9]. The diagonal $\Gamma_{ll}(u_l(t))$ are the *direct transfer operators (or direct transfers)* and the non-diagonal elements $\Gamma_{lk}(u_k(t))$ (with $l \neq k$) are the *cross-coupling transfer operators (or cross-couplings)*. If all the cross-couplings $\Gamma_{lk}(u_k(t))$ ($l \neq k$) are null, then the multivariable hysteresis comes down to several independent monovariable hysteresis and its handling will be easier. In this paper, these cross-couplings are not null, which makes the fundamental challenge of the multivariable case relative to the monovariable one because an input u_k affects an output y_l (where $l \neq k$).

It is important to notice that the structure of the model and thus the identification procedure may differ according if the number m of inputs is similar or not to the number p of outputs in the vector U and vector Y respectively. The following clarification may therefore be useful in the sequel. When $m = p$, the multivariable hysteresis $\Gamma(U(t))$ is square; and when $m \neq p$, it is rectangular. For a rectangular hysteretic system, it is said underactuated if $m < p$ and overactuated if $m > p$. For a square hysteretic system ($m = p$), it is also called fully actuated.

3.2. The multivariable classical Prandtl-Ishlinskii model

Let us now give the definition of a multivariable classical Prandtl-Ishlinskii model.

Definition 3..2: The multivariable classical Prandtl - Ishlinskii model is given by equ 3 where each hysteresis $\Gamma_{lk}(u_k(t))$ is defined by:

$$\Gamma_{lk}(u_k(t)) = \sum_{i=1}^{n_{lk}} w_{lki} \cdot \max\{u_k(t) - r_{lki}, \min\{u_k(t) + r_{lki}, y_{elki}(t-T)\}\}$$

where w_{lki} and r_{lki} are the weighting and the threshold of the i^{th} hysteron of the model that links the output $y_l(t)$ with the input $u_k(t)$, and where $y_{elki}(t-T)$ is the elementary output of the hysteron at time $t-T$. The number of hysterons for the operator $\Gamma_{lk}(u_k(t))$ is given by n_{lk}.

Therefore, each output $y_l(t)$ is given by:

$$y_l(t) = \sum_{k=1}^{m} \Gamma_{lk}(u_k(t)) = \sum_{k=1}^{m} \sum_{i=1}^{n_{lk}} w_{lki} \cdot \max \left\{ \begin{array}{l} u_k(t) - r_{lki}, \\ \min \left\{ \begin{array}{l} u_k(t) \\ +r_{lki}, y_{elki}(t-T) \end{array} \right\} \end{array} \right\} \quad (4)$$

The numbers n_{lk} of hysterons of each operator $\Gamma_{lk}(u_k(t))$ ($l = 1 \cdots p$ and $k = 1 \cdots m$) are independent and thus can be different.

3.3. Parameters identification

In this subsection, we present the identification procedure for the multivariable model $\Gamma(U(t))$. The identified model can be afterwards used to derive the multivariable hysteresis compensator, as we will see in the next section. The operator $\Gamma(U(t))$ contains $p \times m$ components and each component $\Gamma_{lk}(u_k(t))$ ($l = 1 \cdots p$ and $k = 1 \cdots m$) contains n_{lk} thresholds and n_{lk} weightings to be identified. So, the total number of parameters of $\Gamma(U(t))$ to be identified is:

$$2 \times \left(\sum_{l=1}^{p} \sum_{k=1}^{m} n_{lk} \right) \quad (5)$$

in which there are $\sum_{l=1}^{p} \sum_{k=1}^{m} n_{lk}$ weightings and $\sum_{l=1}^{p} \sum_{k=1}^{m} n_{lk}$ thresholds.

If the number of hysterons in each component $\Gamma_{lk}(u_k(t))$ is the same and equal to n, equ 5 becomes:

$$2 \times p \times m \times n \quad (6)$$

The principle of identification in this multivariable case consists in applying the monovariable identification procedure in [22], detailed in the Appendix, to every component $\Gamma_{lk}(u_k(t))$. It is detailed below. The monovariable identification procedure based on the least-square optimization in [18] can also be applied for every component $\Gamma_{lk}(u_k(t))$ but its disadvantage is the high calculation time and cost.

Step.1 - Identification of the parameters of $\Gamma_{11}(u_1(t))$

For that, apply a sine input $u_1(t)$ to the system and leave the remaining inputs $u_k(t) = 0$ ($k = 2 \cdots m$). The output $y_1(t)$ is recorded and the hysteresis of the input-output map $(u_1(t), y_1(t))$ can be plotted. The equation of $y_1(t)$ can also be taken from equ 4 which yields:

$$y_1(t) = \Gamma_{11}(u_1(t)) = \sum_{i=1}^{n_{11}} w_{11i} \cdot \max \left\{ \begin{array}{l} u_1(t) - r_{11i}, \\ \min\{u_1(t) + r_{11i}, y_{e11i}(t-T)\} \end{array} \right\} \quad (7)$$

After choosing the number n_{11} of hysterons, the procedure of monovariable identification described in the Appendix is applied to calculate the weightings w_{11i} and the thresholds r_{11i}.

Step.2 - Identification of the parameters of $\Gamma_{l1}(u_1(t))$ with $l = 2 \cdots p$

In this, the parameters of the couplings transfers $\Gamma_{l1}(u_1(t))$ (with $l = 2 \cdots p$) are identified when an input $u_1(t)$ is applied. For that, when during Step.1 we applied a sine input $u_1(t)$, the other outputs $y_l(t)$ ($l = 2 \cdots p$) should have also been recorded. Then, for each output $y_l(t)$, the hysteresis of the input-output map $(u_1(t), y_l(t))$ can be plotted. In the meantime, the equation of $y_l(t)$ is yielded from equ 4:

$$y_l(t) = \Gamma_{l1}(u_1(t)) = \sum_{i=1}^{n_{l1}} w_{l1i} \cdot \max \left\{ \begin{array}{l} u_1(t) - r_{l1i}, \\ \min\{u_1(t) + r_{l1i}, y_{el1i}(t-T)\} \end{array} \right\} \quad (8)$$

After choosing the number n_{l1} of hysterons, the procedure of monovariable identification described in the Appendix is once again applied to caclulate the weightings w_{l1i} and the thresholds r_{l1i}.

Step.3 - Identification of the parameters of $\Gamma_{kk}(u_k(t))$ with $k = 2 \cdots p$

This step is similar to the step.1 but we apply a sine input $u_k(t)$ ($k \in \{2, 3, \cdots, p\}$) and leave the remaining $u_\theta(t)$, with $\theta \notin \{1, k\}$, equal to zero. Then the input-output map $(u_k(t), y_k(t))$ is plotted and used for the identification. Each $\Gamma_{kk}(u_k(t))$ is a direct transfer. The corresponding equation is taken from equ 4:

$$y_k(t) = \Gamma_{kk}(u_k(t)) = \sum_{i=1}^{n_{kk}} w_{kki} \cdot \max \left\{ \begin{array}{l} u_k(t) - r_{kki}, \\ \min\{u_k(t) + r_{kki}, y_{ekki}(t-T)\} \end{array} \right\} \quad (9)$$

Then, we choose a number n_{kk} of hysterons. Finally, we apply again the procedure of identification for monovariable hysteresis described in the Appendix to derive the weightings w_{kki} and the thresholds r_{kkli}.

Step.4 - Identification of the parameters of $\Gamma_{lk}(u_k(t))$ with $l = 2 \cdots p$

When during the step.3 we applied an input $u_k(t)$, such that $k \in \{2,3,\cdots,p\}$ for over and fully actuated system and $k \in \{2,3,\cdots,m\}$ for underactuated system, we should also record the outputs $y_l(t)$ with $l \in \{1,2,3,\cdots,p\} - \{k\}$. This correponds to the cross-couplings observed at the output $y_l(t)$ when an input $u_k(t)$ is applied, $l \neq k$. Then the input-output map $(u_k(t), y_l(t))$ is plotted and used for the identification. The related equation is taken from equ 4:

$$\begin{aligned} & y_l(t) = \Gamma_{lk}(u_k(t)) \\ & = \sum_{i=1}^{n_{lk}} w_{lki} \cdot \max \left\{ \begin{array}{l} u_k(t) - r_{lki}, \\ \min\{u_k(t) + r_{lki}, y_{elki}(t-T)\} \end{array} \right\} \end{aligned} \tag{10}$$

After choosing a number n_{lk} of hysterons, again the procedure of identification for monovariable hysteresis described in the Appendix is applied to calculate the weightings w_{lki} and the thresholds r_{lki}.

4. A NEW MULTIVARIABLE CLASSICAL PRANDTL-ISHLINSKII COMPENSATOR

In the previous section, the extension of the classical Prandtl-Ishlinskii model into a multivariable model was detailed, along with the identification procedure was carefully presented. In this section, a multivariable compensator for the multivariable classical Prandtl-Ishlinskii model is proposed. The multivariable compensator is valid for square systems of m inputs and m outputs.

4.1. Definition of multivariable compensation

In order to further develop a multivariable compensator, we first give the definition of compensation in multivariable hysteresis. The definition is similar to that of monovariable hysteresis, see [22], but we extend the scalar signals $u(t)$ and $y(t)$ into vector signals $U(t)$ and $Y(t)$. The definition is given for rectangular systems of m inputs and p outputs. Consider Fig. 2 where

$Y_r(t) = \begin{pmatrix} y_{r1}(t) & y_{r2}(t) & \cdots & y_{rp}(t) \end{pmatrix}^T$ is the reference input.

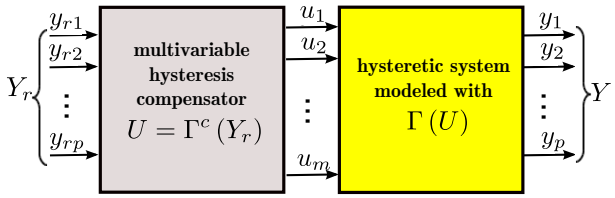

Fig 2: Compensation of a multivariable hysteresis.

Definition 4..1: The exact compensation of the multivariable hysteresis $\Gamma(U(t))$ from the multivariable compensator $\Gamma^c(Y_r(t))$ is obtained when:

$$\begin{aligned} & Y(t) = Y_r(t) \quad \Leftrightarrow \quad Y(t) = \Gamma^c(\Gamma(Y_r(t))) = Y_r(t) \\ & \Leftrightarrow y_l(t) = y_{rl}(t), \text{ with } l = 1 \cdots p, \text{ for } t > t_1 \text{ with } t_1 \geq 0. \end{aligned}$$

Definition 4..2: An approximate compensation for the multivariable hysteresis system is when the compensator $\Gamma^c(Y_r(t))$ yields:

$$\begin{aligned} & Y(t) \simeq Y_r(t) \quad \Leftrightarrow \quad Y(t) \simeq \Gamma^c(\Gamma(Y_r(t))) \simeq Y_r(t) \\ & \Leftrightarrow y_l(t) \simeq y_{rl}(t), \\ & \text{with } l = 1 \cdots p, \text{ for } t > t_1 \text{ with } t_1 \geq 0. \end{aligned}$$

From Def. 4..1 and Def. 4..2, we can conclude that a multivariable compensator permits to have both the cross -couplings rejection and the accuracy: $y_l(t) = y_{rl}(t)$ (or $y_l(t) \simeq y_{rl}(t)$) whatever $y_{r\theta}(t)$, with $\theta \neq l$.

4.2. Useful lemma

The following lemmas will be useful further.

Lemma 4..1: Consider a (monovariable) classical Prandtl -Ishlinskii compensator of input $y_r(t)$ and of output $u(t)$. For a sampling time T that is small enough relative to the period of the input $y_r(t)$, which is considered periodic, we have:

$\left| \frac{\partial u(t)}{\partial y_r(t)} - \frac{\partial u(t-T)}{\partial y_r(t)} \right| \to 0$

where $\frac{\partial u(t)}{\partial y_r(t)}$ is the slope of the map $(y_r(t), u(t))$ describing the compensator.

Proof: See [22]. □

4.3. Formulation of the multivariable hysteresis compensator

We observe from equ 5 that the total number of parameters to be identified increases substantially with the number of degrees of freedom (dof) of the system. Consequently, the complexity of the compensator calculation increases with the number of dof. We propose here a technique that permits to avoid the compensator calculation, which therefore eases the calculation whatever the number of dof. In fact, the principle consists in re-arranging the model Γ to yield the compensator Γ^c. By doing so, as soon as the model is identified, the compensator is directly derived by restructuration.

Consider a square system of m inputs and m outputs. The proposed compensator is given by Theo. 4..1.

Theorem 4..1: The following control law:

$U(t) = \Gamma^c(Y_r(t)) = Y_r(t) + U(t-T) - \Gamma(U(t-T))$

is an approximate multivariable compensator of the multivariable classical Prandtl-Ishlinskii hysteresis model $\Gamma(U(t))$ defined by equ 3 and Def. 3..2.

Proof: Rewrite the model in equ 3 and Def. 3..2 as follows:

$Y(t) = \Gamma(U(t)) = -U(t) + U(t) + \Gamma(U(t))$.

Introduce the proposed compensator in Theo. 4..1 to this model. We obtain:

$Y(t) = Y_r(t) + O$,

where
$O = U(t-T) - U(t) + \Gamma(U(t)) - \Gamma(U(t-T))$.

Let us calculate the derivative of the output $Y(t)$ with respect to the reference input $Y_r(t)$:

$\overrightarrow{\nabla} Y(t) = \overrightarrow{\nabla} Y_r(t) + \overrightarrow{\nabla} O$

where each result of the gradient $\overrightarrow{\nabla} \cdot$ operation gives a $m \times m$ sized matrix.

With regards to $\overrightarrow{\nabla} O$, we have:

$\overrightarrow{\nabla} O = \overrightarrow{\nabla}(U(t-T) - U(t)) + \overrightarrow{\nabla}(\Gamma(U(t)) - \Gamma(U(t-T)))$

where $\overrightarrow{\nabla}(U(t-T) - U(t))$ and $\overrightarrow{\nabla}(\Gamma(U(t)) - \Gamma(U(t-T)))$ are matrices of size $m \times m$ and given by:

$$\overrightarrow{\nabla}(U(t-T) - U(t)) = \left[\frac{\partial u_i(t-T)}{\partial y_{rl}(t)} - \frac{\partial u_i(t)}{\partial y_{rl}(t)}\right]$$

and

$$\overrightarrow{\nabla}(\Gamma(U(t)) - \Gamma(U(t-T))) = \left[\frac{\partial\left(\sum_{k=1}^{m}\Gamma_{ik}(u_k(t))\right)}{\partial y_{rl}(t)} - \frac{\partial\left(\sum_{k=1}^{m}\Gamma_{ik}(u_k(t-T))\right)}{\partial y_{rl}(t)}\right]$$

such as: $i = 1 \cdots m$ is the row index and $l = 1 \cdots m$ is the column index.

On the one hand, since, the models $\Gamma_{ik}(u_k(t))$ are independent of the reference input $y_r(t)$, we have:

$$\left|\frac{\partial\left(\sum_{k=1}^{m}\Gamma_{ik}(u_k(t))\right)}{\partial y_{rl}(t)} - \frac{\partial\left(\sum_{k=1}^{m}\Gamma_{ik}(u_k(t-T))\right)}{\partial y_{rl}(t)}\right| \to 0; \quad \forall i; \quad \forall l$$

On the other hand, respecting the condition on the sampling time T, from Lemma. 4..1, we can yield that:

$$\left|\frac{\partial u_i(t-T)}{\partial y_{rl}(t)} - \frac{\partial u_i(t)}{\partial y_{rl}(t)}\right| \to 0; \quad \forall i; \quad \forall l$$

With regards to $\overrightarrow{\nabla} Y_r(t)$, we have:

$\overrightarrow{\nabla} Y_r(t) = I_{m\times m}$

where $I_{m\times m}$ is the eye matrix of size $m \times m$.

Consequently:

$\overrightarrow{\nabla} Y(t) = I_{m\times m} + \overrightarrow{\nabla} O \simeq I_{m\times m}$

which implies:

$Y(t) \simeq Y_r(t)$.

From Def. 4..2, we therefore conclude that the control law in Theo. 4..1 provides an approximate compensation of the classical Prandtl-Ishlinskii model. □

Fig. 3 depicts the block diagram of the multivariable compensator $\Gamma^c(Y_r(t))$ implemented to control the square system modeled by $\Gamma(U(t))$. Notice that there is a (nonlinear) feedback inside the compensator. Such structure is called inverse multiplicative: *inverse* because of the feedback, and *multiplicative* because the compensator is in cascade with the system.

5. APPLICATION TO THE CONTROL OF A 2-DOF PIEZOELECTRIC ACTUATOR

In this section, we apply the developed multivariable modeling, identification and compensation techniques to feedforward control the displacement (bending) of a two degrees of freedom piezoactuator.

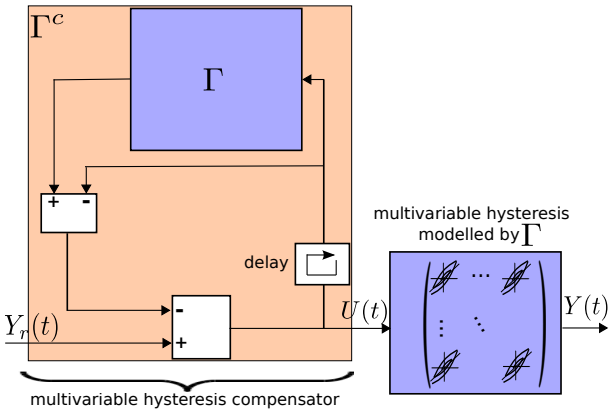

Fig 3: Diagram showing the implementation of the multivariable compensator.

5.1. Presentation of the experimental setup

The actuator to be modeled and controlled is a clamped-free piezoelectric cantilever with rectangular structure. Fig. 4-a depicts a schematic view of the piezoactuator. It is composed of two piezoelectric layers: upper layer and lower layer. The interface between the two layers is based on silver material and serves as ground electrode. There are two electrodes in the upper surface and two other electrodes in the lower surface of the actuator. They are also based on silver materials. Fig. 4-b depicts the front view. We can observe from this view the four electrodes that are denoted by U_1, U_2, U_3 and U_4. The poling direction P in each piezoelectric layer is as indicated in the same figure.

When a positive voltage u_x is applied to U_1 and to U_3, the resulting electrical fields between U_1 and the ground and between U_3 and the ground are in the same direction than the poling which yields an expansion of the corresponding sectors along z-axis (see Fig. 4-c). In the meantime, if we apply the opposite voltage $-u_x$ to U_2 and U_4, the electrical fields between these two latter electrodes and the ground are in the opposite direction of the poling which results in a contraction of the corresponding sectors. This expansion and contraction along z will yield a bending of the overall cantilever along x-axis as depicted in Fig. 4-d. If u_x is negative, and thus $-u_x$ positive, the bending of the actuator will be in the opposite direction.

Now, if we apply a positive voltage u_y to electrodes U_3 and U_4 and a negative voltage $-u_y$ to electrodes U_1 and U_2, an expansion of the lower layer and a contraction of the upper layer along z-axis are obtained (Fig. 4-e) and an overall bending of the cantilever along y-axis is resulted (Fig. 4-f). Again, to reverse the direction of the bending, we use a negative u_y instead of a positive value.

From the principle explaind above, the actuator can be considered as a system with two inputs rassembled in a

vector $U(t) = (u_x(t), u_y(t))^T$ and two outputs rassembled in a vector $Y(t) = (x(t), y(t))^T$. Due to the fabrication imprecision, the actuator is not really symmetrical relative to the y-axis in Fig. 4-b. Therefore this generates cross-couplings: a voltage u_x will induce slight displacement along the y-axis and a voltage u_y will induce displacement along the x-axis. Furthermore, the electrical fields are not purely vertical between the upper or lower electrodes and the ground electrode and, as a consequence, the unwanted deformed fields within the layers will generate additional cross-couplings. A physical modeling of these misalignment and electrical fields would yield a full model utilizable for a design point of view. However, such model would be too complex and less utilizable in a control point of view. A black-box model such as the suggested multivariable classical Prandtl-Ishlinskii is therefore well convenient for that.

The principle of this actuator has been patented in [36]. In [37], we used a version with 36 layers of this actuator: 18 layers for the above side of the ground-electrode and 18 for the lower side. This permits to work at low voltage for the same displacement. This multilayered actuator will be used in the rest of this paper. It is worth to note that the actuator is well appreciated for microrobotic precise positioning applications [1].

The experimental setup is composed of the piezoactuator itself, with diemnsions of $27mm \times 1mm \times 1mm$. The active length, i.e. the non-clamped part of the cantilever, is of $24mm$. The material that composes the layers of the actuator is the PZT ceramics (lead zirconate titanate). Two inductive sensors (ECL202 from *IBS* company) are used to measure the displacements x and y. In this experiment, they are set to have a resolution of $40nm$, a range of $\pm 250\mu m$ and a bandwidth of $2kHz$ which are sufficient enough to track the performances of the actuator. A polymer cube wrapped with aluminium sheet and placed on the top of the piezoactuator permits to the sensors to measure the displacements, as the sensors require a sensitive reflector. The distance that separates the two sensors are sufficiently large relative to the interference distance of their magnetic signals. Thus, they can work independently without magnetic fields interference. It is worth to note that the sensors are used to characterize the actuator and to validate the feedforward control performances. The feedforward control itself does not require sensors for feedback, which constitutes one of its major advantages. We employ a computer and a dSPACE board to manage the signals (driving inputs $u_x(t)$ and $u_y(t)$, measured outputs $x(t)$ and $y(t)$) and to implement the controller thanks to MATLAB-SIMULINK. The sampling period T is set equal to $50\mu s$ for all the experiments, which is largely sufficient for the characterization and control carried out in this paper. As the actuator works at low voltage ($\pm 10V$) and does

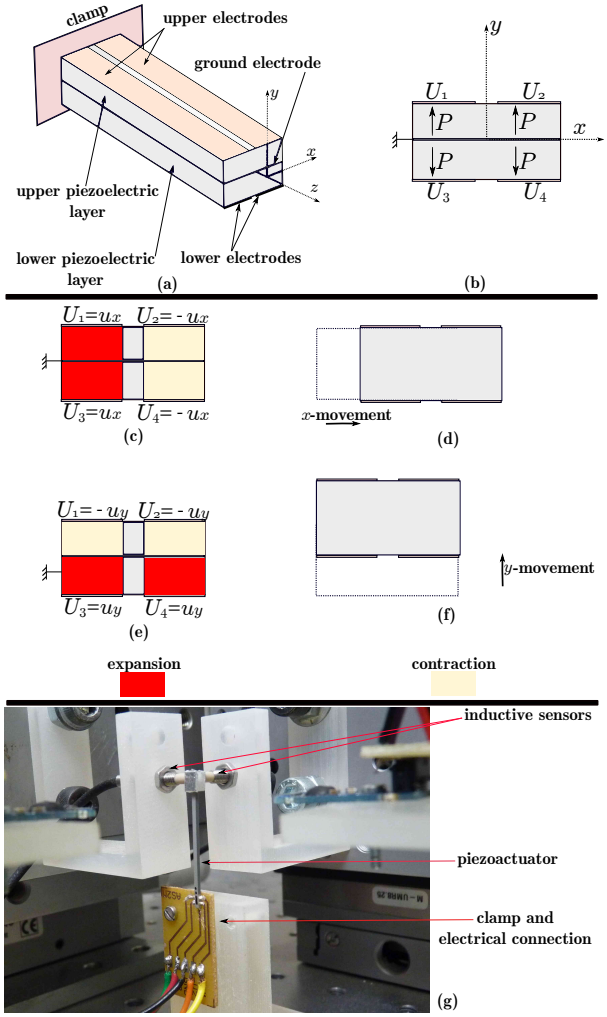

Fig 4: The experimented piezoactuator. (a) and (b): perspective and front views of the actuator. (c) and (d): obtention of the x movement from the actuator. (e) and (f): obtention of the y movement from the actuator. (g): a photography.

not require high current, there is no need of voltage or power amplifiers. The driving voltages from the dSPACE aquistion board are directly sent to the actuator. Fig. 4-c is a photography of the clamped-free piezoactuator and of the sensors.

5.2. Hysteresis and cross-couplings characterization

This subsection is devoted to the characterization of the piezoactuator. The characterization is carried out with a sine input voltage $u_k(t) = \hat{u}_k sin(2\pi f_k t)$ $(k \in \{x, y\})$. The amplitude $\hat{u}_k$ is chosen to cover the maximal range of use. Notice that higher this amplitude is, stronger will be the hysteresis. Since the classical Prandtl-Ishlinskii model is rate-independent, a model will only be valid for a single frequency, which is the frequency f_k used for the characterization and for the identification. In addition, this frequency should not be too high in order to avoid the

phase-lag. Thus it is generally taken much lower than the bandwidth of the process [6]. In counterpart, very low frequency can be used which makes possible the consideration of eventual creep nonlinearity [38] by the classical Prandtl-Ishlinskii approach and its extension into multivariable. In the rest of the section, we will work with four frequencies ($50Hz$, $100Hz$, $150Hz$ and $200Hz$) which are sufficiently high for various applications such as microrobotic precise positioning.

First a sine input voltage $u_x(t)$ with an amplitude of $10V$ and a frequency of $50Hz$ is applied. The remaining input voltage is set equal to zero: $u_y(t) = 0$. The resulting displacements $x(t)$ and $y(t)$ are recorded. Fig. 5-a (solid-line) depicts the hysteresis in the $(u_x(t), x(t))$ map (direct hysteresis) and Fig. 5-c (solid-line) depicts the hysteresis in the $(u_x(t), y(t))$ map (cross-coupling along y-axis). Then, we set $u_x(t) = 0$ and we apply a sine input voltage $u_y(t)$ with an amplitude of $10V$ and a frequency of $50Hz$. Again, the resulting outputs $x(t)$ and $y(t)$ are reported. Fig. 5-b (solid-line) depicts the hysteresis in the $(u_y(t), x(t))$ map (cross-coupling along x-axis) and Fig. 5-d (solid-line) depicts the hysteresis in the $(u_y(t), y(t))$ map (direct hysteresis). These results show the strong hysteresis of the piezoactuator. They show that the direct hysteresis have an amplitude in excess of $\frac{h}{H} = \frac{2\times 10\mu m}{2\times 58\mu m} = 17\%$ and of $\frac{h}{H} = \frac{2\times 8\mu m}{2\times 50.5\mu m} = 15.8\%$ over the operating range for x and y axis respectively. We also observe the existence of the cross-couplings with range of $H_c = 2\times 1.5\mu m = 3\mu m$ and $H_c = 2\times 2\mu m = 4\mu m$ along x and y axis respectively. Observe that these cross-couplings are also hysteresis.

Then, the same characterization than the previously presented (by utilizing $f_k = 50Hz$) is effectuated but with a frequency of $100Hz$, $150Hz$ and $200Hz$ successively. The results are presented in Fig. 5: dashed-line for $100Hz$, dashed-o for $150Hz$ and dashed-x for $200Hz$. As we can observe, by increasing the frequency, the shape of the hysteresis is also modified (rate-dependency). First the amplitude h of the hysteresis increases. Then, from certain frequency, the extremities of the curve, called turning-points, become rounded which informs us that the phase-lag starts to be involved. These characterizations show that the actuator exhibits bi-variable (two-input-two-output) hysteresis nonlinearity: important cross-couplings with hysteresis shape, and important hysteresis amplitudes in the direct transfers. As mentionned above, due to the rate - independency of the bivariable classical Prandtl-Ishlinskii model, a model identified from one frequency, let us say $f_k = 50Hz$, will not be valid for the hysteresis with the other frequencies. However, in the next section, we will identify a model from $f_k = 50Hz$ and will evaluate its precision to track other hysteresis at different frequencies ranging between $10Hz$ and $420Hz$. Notice that the bandwidth of the piezoactuator employed in this paper was identified as between $400Hz$ and $500Hz$ for the two axes [37]. Therefore, the range of frequency for the analysis carried out includes a phase-lag domain.

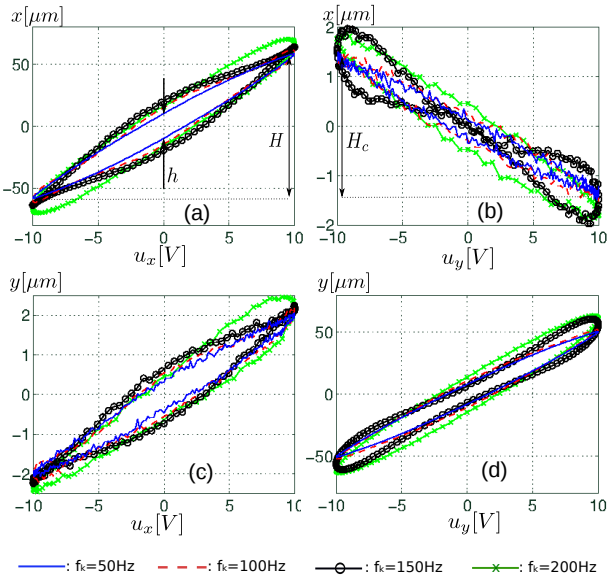

Fig 5: Hysteresis and cross-couplings at different frequencies f_k.

5.3. Modeling, parameters identification and model precision evaluation

In this section, we will identify the bivariable classical Prandtl-Ishlinskii model with the experimental curves obtained at $f_k = 50Hz$. Then we will verify its validity with lower voltage amplitudes (minor loops). We will also evaluate the precision of the identified rate-independent model when other frequencies from $10Hz$ to $420Hz$ of the voltage are used to drive the process.

Let equ 11 be the model of the piezoactuator where $\Gamma_{lk}(u_k(t))$ ($l \in \{x,y\}$ and $k \in \{x,y\}$), defined in Def. 3..2, are to be identified.

$$Y(t) = \begin{pmatrix} x(t) \\ y(t) \end{pmatrix} = \Gamma(U(t)) = \begin{pmatrix} \Gamma_{xx}(u_x(t)) + \Gamma_{xy}(u_y(t)) \\ \Gamma_{yx}(u_x(t)) + \Gamma_{yy}(u_y(t)) \end{pmatrix} \quad (11)$$

Following the procedure detailed in Section. 3.3., the parameters of the direct transfer $\Gamma_{xx}(u_x(t))$ are first identified by utilizing the experimental curve of Fig. 5-a (solid-line) and the monovariable identification procedure in the Appendix. This corresponds to step.1. Then, step.2 permits to identify the parameters of the cross-coupling $\Gamma_{yx}(u_x(t))$ by using the experimental curve in Fig. 5-c (solid-line). Afterwards, we identify the parameters of the direct transfer $\Gamma_{yy}(u_y(t))$ with the experimental curve in Fig. 5-d (solid-line) which correponds to step.3. Finally, parameters of the cross-coupling $\Gamma_{xy}(u_y(t))$ are identified by using the

experimental curve in Fig. 5-b (solid-line) which corresponds to step.4. We choose the same number of hysterons: $n = 15$, for the four hysteresis models. In fact, above $n = 15$, the precision of the models stops to increase substantially. The identified parameters are:

$$r_{lk} = \begin{pmatrix} 0.07 & 0.32 & 0.74 & 1.3 & 2 & 2.8 \\ 3.67 & 4.61 & 5.54 & 6.5 & 7.34 & 8.1 & 8.8 & 9.3 & 9.7 \end{pmatrix} \quad (12)$$

and

$$w_{xx} = \begin{pmatrix} 4.3 \\ -3.95\times10^{-1} \\ 1.17\times10^{-1} \\ 6.57\times10^{-1} \\ 2.07\times10^{-1} \\ 2.52\times10^{-1} \\ 6.05\times10^{-1} \\ 1.5\times10^{-1} \\ 2.65\times10^{-1} \\ 2.29\times10^{-1} \\ 2.07\times10^{-1} \\ 3.81\times10^{-1} \\ 4.11\times10^{-1} \\ 2.56\times10^{-1} \\ 2.28 \end{pmatrix} \quad w_{xy} = \begin{pmatrix} 2.77\times10^{-1} \\ -7.38\times10^{-2} \\ -1.62\times10^{-1} \\ 2.34\times10^{-1} \\ -3.12\times10^{-1} \\ 2.11\times10^{-1} \\ -4.17\times10^{-2} \\ 3.86\times10^{-2} \\ -8.75\times10^{-2} \\ 1.45\times10^{-1} \\ -1.31\times10^{-1} \\ 8.36\times10^{-2} \\ -9.6\times10^{-2} \\ 7.3\times10^{-2} \\ 2.68\times10^{-2} \end{pmatrix}$$

$$w_{yx} = \begin{pmatrix} 1.84\times10^{-1} \\ -3.69\times10^{-2} \\ -6.64\times10^{-2} \\ 6.15\times10^{-2} \\ 8.57\times10^{-2} \\ -8.09\times10^{-2} \\ 4.19\times10^{-2} \\ 3.77\times10^{-2} \\ -6.97\times10^{-2} \\ 6.2\times10^{-2} \\ 3.28\times10^{-2} \\ 6.39\times10^{-2} \\ -1.75\times10^{-1} \\ 2.33\times10^{-1} \\ 1.65\times10^{-1} \end{pmatrix} \quad w_{yy} = \begin{pmatrix} 3.63 \\ 7.86\times10^{-2} \\ 9.17\times10^{-3} \\ 2.55\times10^{-1} \\ 3.49\times10^{-1} \\ 4.24\times10^{-1} \\ 1.07\times10^{-1} \\ 1.8\times10^{-1} \\ 2.88\times10^{-1} \\ 2.04\times10^{-1} \\ 2.52\times10^{-1} \\ 1.44\times10^{-1} \\ 6.97\times10^{-1} \\ -1.51\times10^{-1} \\ 9.7\times10^{-1} \end{pmatrix} \quad (13)$$

Remark 5..1: In this modeling, we have chosen to have the same thresholds vector for the four hysteresis $\Gamma_{lk}(u_k(t))$ ($l \in \{x,y\}$ and $k \in \{x,y\}$). This is because the voltages $u_x(t)$ and $u_y(t)$ utilized for the characterization and identification have the same amplitude $10V$. The chosen partition in equ 12 has been yielded with a uniform time-domain partition of the input voltage $u_k(t) = \hat{u}_k sin(2\pi ft)$. Although, it is possible to use a uniform partition in the $u_k(t)$ domain, i.e. over the range $-10V \rightarrow 10V$. In our case, creating the partition in the time-domain was more simple because of the experimental data defined and presented in the time-domain format. Non-uniform partitions are also possible instead of uniform ones in the time-domain or in the voltage-domain. Non-uniform and uniform partitions will yield precise models if the number of hysterons $n_{lk} = n$ is high. In counterpart, if $n_{lk} = n$ is low, the different models with different types of partition may yield different precisions. As far as we know, there is no further analysis permitting to precisely evaluate the performances of a classical Prandtl-Ishlinskii model versus the partitions chosen and this is out of the scope of this paper.

Fig. 6 show the comparison between the experimental hysteresis and the simulation of the above identified model, all at frequency $f_k = 50Hz$. The figures show that the identified model is convenient enough to track the hysteresis. In the direct transfers (Fig. 6-a and d), (experimental and model simulation) hysteresis with voltages of amplitude equal to $5V$ have also been added. These internal loops demonstrate that the identified model is still precise.

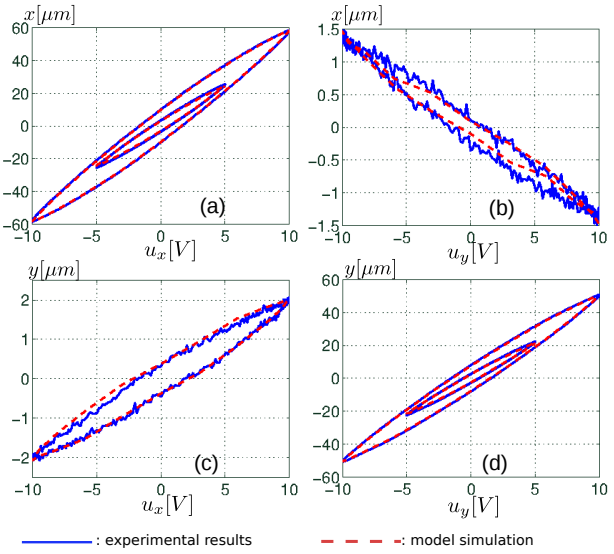

Fig 6: Experimental results and model simulation.

Now, let us evaluate the above identified model (identified at $f_k = 50Hz$) when the experimental hysteresis are obtained at different frequencies ranging between $10Hz$ and $420Hz$. The aim is to evaluate the precision of the rate-independent hysteresis model when the excition frequency is different from the frequency of identification. Fig. 7 present the RMS-error between the model simulation and the experiments *versus* the excitation frequency. For each of curves (a), (b), (c) and (d) in the figure, the RMS error used for the measure is defined by:

$$RMS_{error\_model} = \sqrt{\frac{1}{N_{exp}} \sum_{j=1}^{N_{exp}} \left(Y_l^{exp}(j) - \Gamma_{lk}\left(u_k^{exp}(j)\right)\right)^2},$$

where Y_l^{exp} ($Y_l^{exp} \in \{x^{exp}, y^{exp}\}$) stands for the experimen-

tal output displacement, u_k^{exp} is the experimental input voltage, N_{exp} is the number of points in the experimental data, and Γ_{lk} is the previously identified model (see equ 11).

The results clearly confirm the rate-independency of the classical Prandtl-Ishlinskii model: the RMS error increases when the excitation frequency is higher than the identification frequency. When the former is lower than the latter, the RMS error remains weak and almost similar to that of $50Hz$. In fact, as long as the excitation frequency is much lower than the bandwidth, the change on the hysteresis curves is not important. This makes therefore the model identified at $50Hz$ almost valid for hysteresis obtained between $10Hz$ and $50Hz$. However, if the excitation frequency is too low (under $0.05Hz$ for instance), the RMS-error will again be increased because of the presence of the creep nonlinearity. The classical Prandtl-Ishlinskii model should be re-identified if the application requires to work at such low frequency. In fact, the creep behaves like a hysteresis at such frequency and has a different shape than the hysteresis between $10Hz$ and $50Hz$. Hence, the model identified at $50Hz$ will not necessarily be valid for a hysteresis (more precisely for the creep) at $0.05Hz$. Contrary to the phase-lag, the hysteresis shape in the creep does not have a rounded turning-points making still possible the use of the classical Prandtl-Ishlinskii model to approximate this.

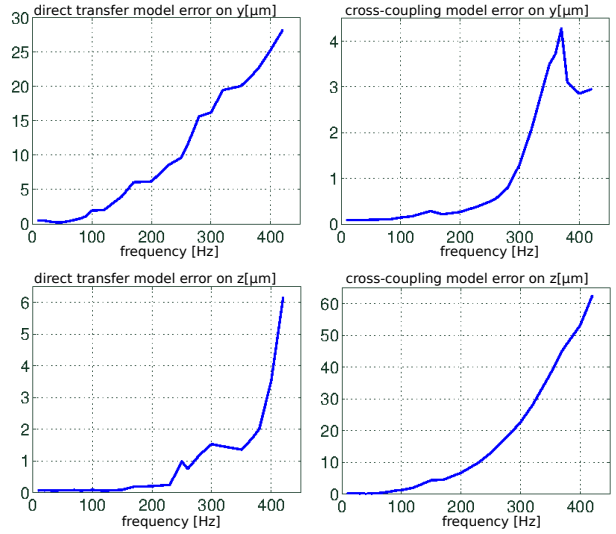

Fig 7: RMS evaluation of the error between the identified model at $f_k = 50Hz$ and the experiments when the frequency of the driving voltages signal is varied.

5.4. Results with the new compensator

In the previous section, we have identified the parameters of the model $\Gamma(U(t))$ by using the experimental data with frequency $f_k = 50Hz$. In this section, we will construct a compensator by utilizing Theo. 4..1 based on that model. Then, different reference tarjectories $Y_r(t) = (x_r(t), y_r(t))^T$ are tested and the tracking performances evaluated.

Verification of the compensated hysteresis and of the reduced cross-couplings

The first experiments consist in verifying if the hysteresis in the direct transfers are linearized and if the cross-couplings are removed. For that, sine reference input $Y_r(t)$ is applied and the input-output $(Y_r(t), Y(t))$ map is afterwards plotted. The amplitude ($50\mu m$) of the reference was chosen to not exceed the maximal range of output during the characterization and identification. As the model has been identified (and thus the compensator calculated) with the experimental data having a frequency of $f_k = 50Hz$, we choose the same frequency for the sine reference signal. Fig. 8-a and c (solid-line) give the $(x_r(t), x(t))$ map (direct transfer) and the $(x_r(t), y(t))$ map (cross-coupling) respectively along x-axis while Fig. 8-b and d (solid-line) give the cross-coupling $(y_r(t), x(t))$ and the direct transfer $(y_r(t), y(t))$ results respectively along y-axis. These figures demonstrate that the hysteresis in the direct transfers which were initially of 17% and 15.8% (see Fig. 5-a and d (solid-line)) are completely linearized (Fig. 8-a and d (solid-line)). We also observe the substantial reduction of the cross-couplings from $\pm 1.5\mu m$ and $\pm 2\mu m$ (Fig. 5-b and c (solid-line)) to about $\pm 0.2\mu m$ and $\pm 0.25\mu m$ respectively (Fig. 8-b and c (solid-line)). These first results demonstrate the efficiency of the proposed technique to compensate for the hysteresis and to reduce the cross-couplings in multiple axis actuator.

Let us now re-identify the model $\Gamma(u(t))$ at an identification frequency of $f_k = 100Hz$ and derive the corresponding compensator by employing Theo. 4..1. Once again, the compensator is applied to the two-axes piezoactuator. Then, let us apply a sine reference signal $Y_r(t)$ with still an amplitude of $50\mu m$, but with an excitation frequency of $100Hz$. The experimental results are in dashed-line of the Fig. 8. They show that the performances are still similar to that with the compensator based on a model identified at $f_k = 50Hz$ previously presented.

The same procedure than with $50Hz$ and with $100Hz$ is repeated at higher frequency: we identify a model $\Gamma(u(t))$ with the experimental hysteresis curves obtained at $f_k = 150Hz$ and then we employ a compensator calculated from this newly identified model to control the piezoactuator. Afterwards an excitation ferquency similar to the identification frequency is used for the sine reference input $Y_r(t)$: $150Hz$. The results are in dashed-o of the Fig. 8. They show that even if the hysteresis in the direct transfers are still linearized, the precision starts to be lost: the gain is not anymore unitary but slightly higher. In addition, the residual cross-couplings start to increase, in particular for the x-axis. The same remarks are observed when the model is identified with experimental curves obtained at $f_k = 200Hz$, when the corresponding compensator is

applied and when a reference signal $Y_r(t)$ of frequency $200Hz$ is applied: see dashed-x of Fig. 8. In fact this reduction of the compensation efficiency at high frequency, even if we use the same frequency for the identification and for the excitation, is due to the round-shaped turning-points of the initial hysteresis which the model could not track, and thus the compensator cannot account for.

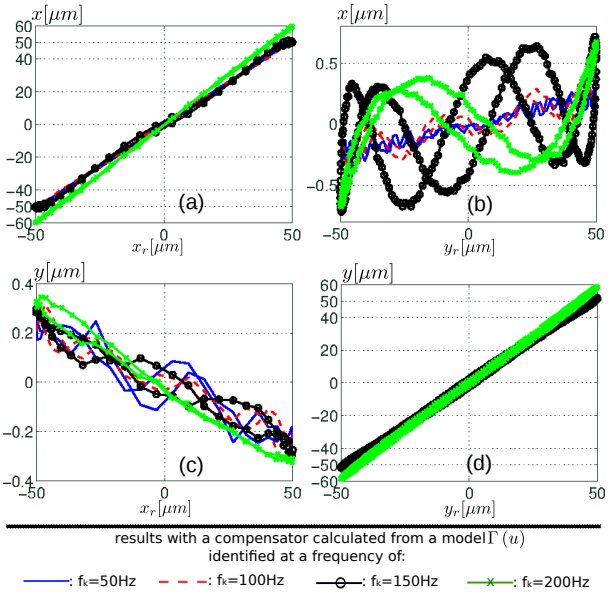

Fig 8: Verification of the compensated hysteresis and of the reduced cross-couplings when using a compensator calculated with a model $\Gamma(u(t))$ identified from different hysteresis frequencies f_k, the excitation frequency being the same than the identification frequency.

Tracking error analysis and cross-couplings analysis

The four previous compensators calculated at the different identification frequency ($f_k = 50Hz$, $f_k = 100Hz$, $f_k = 150Hz$ and $f_k = 200Hz$) are now tested individually when the excitation frequency, i.e. frequency of the sine reference input $Y_r(t)$, is varied from $10Hz$ to $420Hz$. As measure, we use the following RMS error between the reference input and the output of the controlled process: $RMS_{error\_comp} = \sqrt{\frac{1}{N_{exp}} \sum_{j=1}^{N_{exp}} (Y_{rl}(j) - Y_l(j))^2}$, where $Y_{rl} \in \{x_r, y_r\}$ stands for the reference input, $Y_l \in \{x, y\}$ stands for the experimental output and N_{exp} is the number of points in the experimental data.

The results obtained from the compensator calculated at $f_k = 50Hz$ are displayed as the solid-line curves of the Fig. 9. The results from the compensator calculated at $f_k = 100Hz$ are the dashed-line in the same figure, the results from the compensator calculated at $f_k = 150Hz$ are the dashed-o curves and finally the results from the compensator calculated at $f_k = 200Hz$ are the dashed-x curves. The direct transfers (x_r, x) and (y_r, y) along the x and the y axis respectively are displayed in Fig. 9-a and d, whilst the cross-couplings (y_r, x) and (x_r, y) of the same axes are in Fig. 9-b and c respectively.

In order to demonstrate the efficiency of the new multivariable modeling and compensation of hysteresis, we also carried out experiments with existing method of compensation and further do performances comparison. For that, we consider the existing monovariable compensator from [20], then we apply this to control the x-axis and to control the y-axis as if the process was two monovariable systems. The identification and calculation of the two monovariable compensators were carried out with the initial direct hysteresis curves obtained at $50Hz$, i.e. with Fig. 5-a and d (solid-line). The experimental RMS error of compensation with this approach is displayed as the dashed-dot curves in Fig. 9.

As we can see from these different results, the proposed compensator calculated at lower frequencies ($f_k = 50Hz$ and $f_k = 100Hz$) presents the best general performances for the spanned excitation frequency and for the different transfers: the error of linearization (Fig. 9-a and d) are minimized and the reduction of the cross-couplings (Fig. 9-b and c) are maximized with the related compensators. We can particularly appreciate their efficiency even if the excitation frequency is lower than the identification frequency (from $10Hz$ to $50Hz$ and from $10Hz$ to $100Hz$ respectively). We also observe that if the compensator is calculated at high frequency ($f_k = 150Hz$ and $f_k = 200Hz$), the error of compensation is higher when the excitation frequency is lower than the identification frequency f_k, specifically in the direct transfers (Fig. 9-a and d). In fact, as mentionned above, the experimental hysteresis at $150Hz$ and $200Hz$ are affected by the phase-lag and consequently the model (resp. the compensator) will be less precise (resp. efficient). The results also show that the existing compensation method from [20], in dashed-dot curves, cannot account for the cross-couplings since these latters are not reduced (Fig. 9-b and c (dashed-dot)). One of the main advantages of the proposed approach in this paper is therefore the fact that we also reduce the cross-couplings additionally to the hysteresis linearization. Finally, as a last remark, for all the different compensators implemented, when the excitation frequency is above the identification frequency, the RMS-error increases substantially. This substantial increase is due to the phase-lag which becomes more and more important.

In the rest of the experiments, we will use the compensator calculated at the identification frequency of $f_k = 50Hz$ and which show very interesting performances at lower and at slightly higher excitation frequency than f_k.

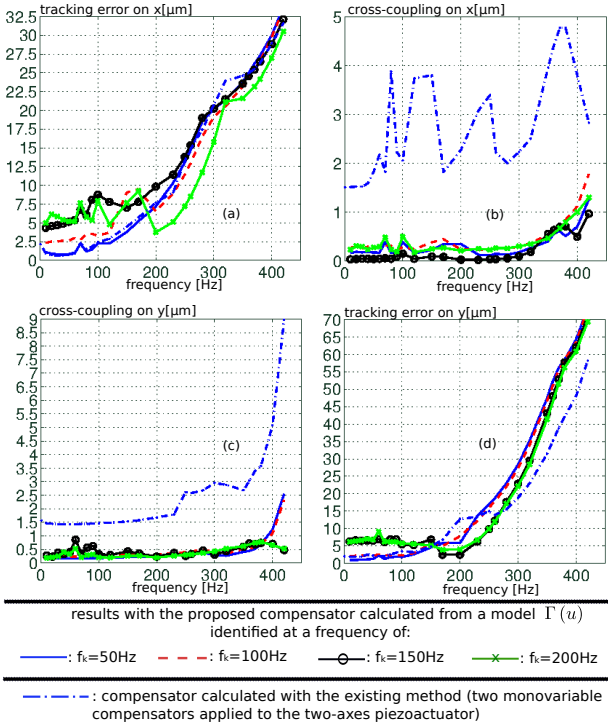

Fig 9: Tracking error ((a) and (d)) and cross-couplings analisys ((c) and (d)) wrt the excitation frequency when using the different compensators calculated.

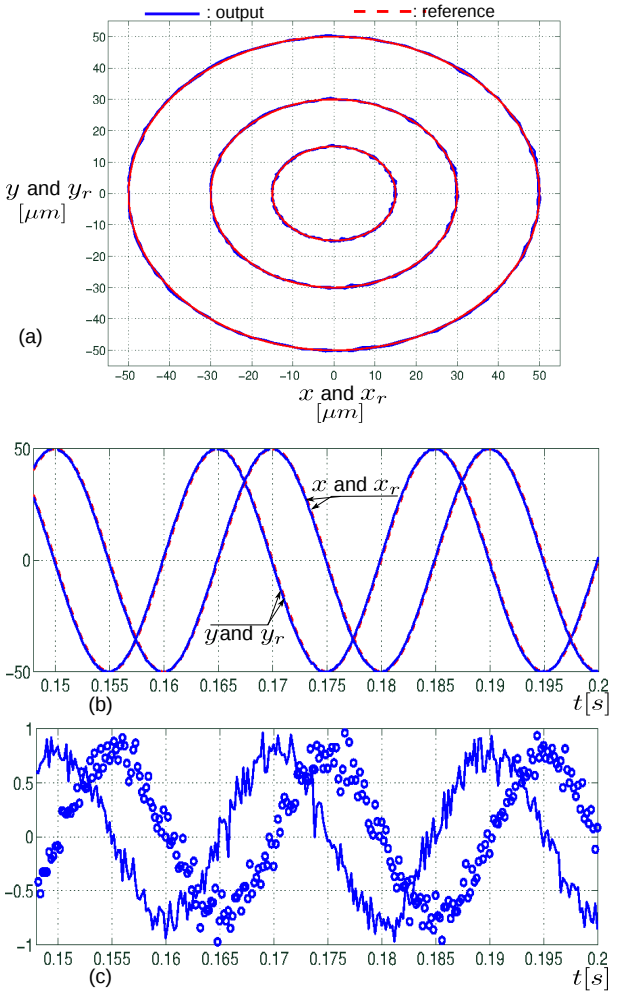

Fig 10: Tracking of circular trajectories.
(a): circular curves with reference radius equal to $15\mu m$, $30\mu m$ and $50\mu m$, solid-lines (—) are the circular outputs whilst dashed-lines (- -) are the circular references. (b): time domain tracking curves where solid-lines (—) are the outputs $x(t)$ and $y(t)$ whilst dashed-lines (- -) are the references $x_r(t)$ and $y_r(t)(t)$. (c): tracking errors where solid-line curve (—) is the tracking error along x-axis and the o-curve (o o o) is tracking error along y-axis, both with reference inputs $x_r(t)$ and $y_r(t)$ of $50\mu m$ amplitude.

Tracking of circular trajectories

In the previous experiments, only one reference, i.e. only $x_r(t)$ or only $y_r(t)$, was applied to the compensated system. Here, both signals are simultaneously applied and a circular trajectory is utilized as spatial reference. The objective is to verify the efficiency of the compensator when references $x_r(t) = \hat{x}_r cos(2\pi ft + \phi)$ and $y_r(t) = \hat{y}_r sin(2\pi ft + \phi)$ are simultaneous. The trajectory frequency f is taken equal to the excitation frequency: $f = f_k = 50Hz$ which is significantly high for such complex trajectory. Different radius $\sqrt{\hat{x}_r^2 + \hat{y}_r^2}$ of the spatial circle have been used ($15\mu m$, $30\mu m$ and $50\mu m$). Fig. 10-a depict the experimental results in the spatial domain. Also, Fig. 10-b and c depict the corresponding inputs and output results in the time-domain and the tracking error respectively, when the radius is $50\mu m$. We use as measure for the tracking error the following formula: $\varepsilon(t) = sgn(\theta)\sqrt{\theta}$, with $\theta = \Big((x_r(t) + y_r(t))^2 - (x(t) + y(t))^2\Big)$. These results demonstrate the capacity of the compensator to still reject the cross-couplings and to track the reference trajectory. All the results present a maximal absolute error $|\varepsilon(t)|$ that does not exceed $1\mu m$, which is $\frac{1\mu m}{50\mu m} = 2\%$ only. Notice that the error $\varepsilon(t)$ includes the error of hysteresis compensation in the direct transfers and the residual cross-couplings.

Tracking of spiral trajectory

A spatial spiral trajectory is now used as reference. The time-domain references are governed by the following equations: $x_r(t) = \hat{x}_r e^{\frac{-t}{\tau}} cos(2\pi ft + \phi)$ and $y_r(t) = \hat{y}_r e^{\frac{-t}{\tau}} sin(2\pi ft + \phi)$, in which the amplitudes are $\hat{x}_r = \hat{y}_r = 50\mu m$ and the frequency still equal to the excitation frequency $50Hz$, which is also considered as significantly high for the complex trajectory studied. During the experiments, first a circular trajectory is run and then a manual trigger is used to start the exponential decay. Fig. 5-a, b and c present the

resulting spatial domain curves, the time domain curves, and the tracking error $\varepsilon(t)$ respectively. As from these results, we observe the good tracking performances and still a maximal absolute error of 2%.

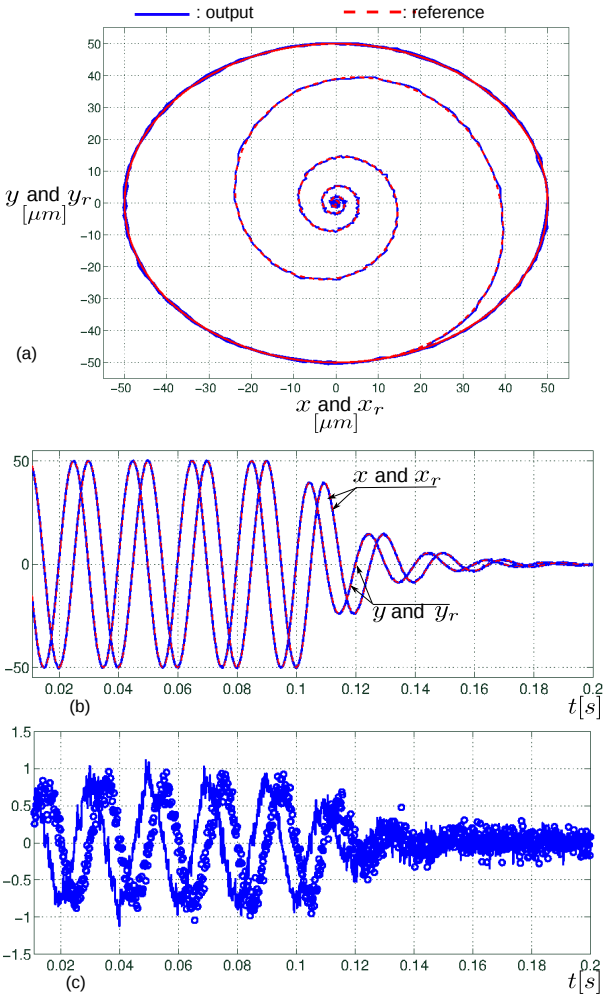

Fig 11: Tracking of spiral trajectory.
(a): spiral curve, solid-line (—) is the spiral output whilst dashed-line (- -) is the spiral reference. (b): time domain tracking curves where solid-lines (–) are the outputs $x(t)$ and $y(t)$ whilst dashed-lines (- -) are the references $x_r(t)$ and $y_r(t)$. (c): tracking error.

Tracking of Lissajous trajectories

The last experiments consist in utilizing more complex trajectory. Lissajours curves have been considered as interesting reference signal for certain applications of piezoelectric actuators such as piezotubes in high speed scanning in atomic force microscopy [39]. Let us use such Lissajous reference to the controlled piezoactuator. The spatial Lissajous reference is governed by the following time-domain references: $x_r(t) = \hat{x}_r cos(2\pi f_x t + \phi)$ and $y_r(t) = \hat{y}_r sin(2\pi f_y t + \phi)$, where $r_f = \frac{f_x}{f_y}$ is the Lissajous ratio. A ratio of $r_f = 1$ gives a circular trajectory, whilst a ratio $r_f > 1$ means that there are more back-and-forth performed along the x-axis than along the y-axis within a same time period. Fig. 12 present the results (spatial domain, time domain and error $\varepsilon(t)$) when utilizing an amplitude $\hat{r}_x = \hat{r}_y = 50\mu m$ and a Lissajous ratio of $r_f = \frac{f_x}{f_y} = \frac{50Hz}{33.33Hz} = \frac{3}{2}$ and Fig. 13 when the Lissajous ratio is $r_f = \frac{f_x}{f_y} = \frac{40Hz}{30Hz} = \frac{4}{3}$. The different experiments also show that the piezoactuator well tracks the complex trajectory at different conditions while still maintaining a negligible maximal absolute error ($|\varepsilon(t)| \approx 2\mu m$).

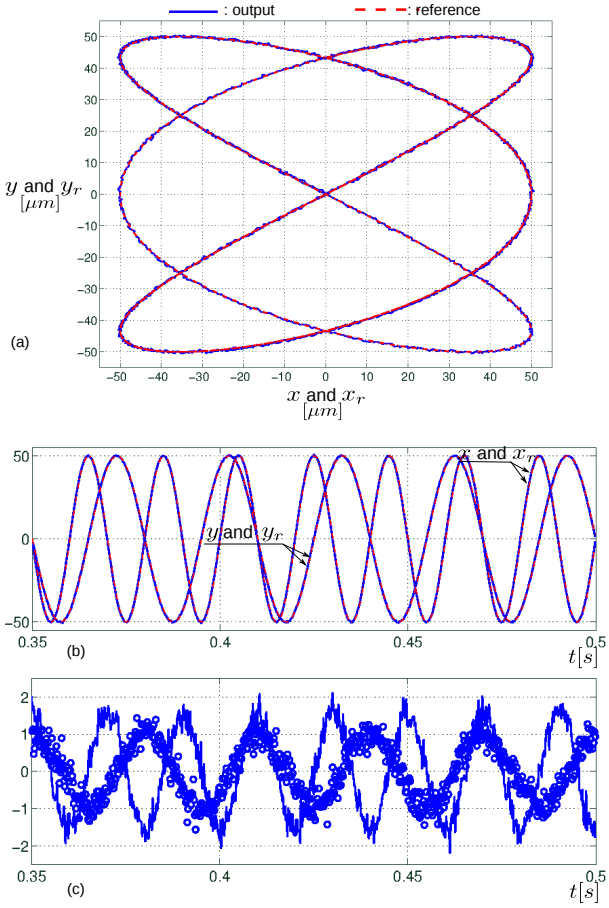

Fig 12: Tracking of Lissajous trajectory with a ratio of $r_f = \frac{3}{2}$.
(a): Lissajous curve, solid-line (—) is the Lissajous output whilst dashed-line (- -) is the Lissajous reference. (b): time domain tracking curves where solid-lines (—) are the outputs $x(t)$ and $y(t)$ whilst dashed-lines (- -) are the references $x_r(t)$ and $y_r(t)$. (c): tracking error.

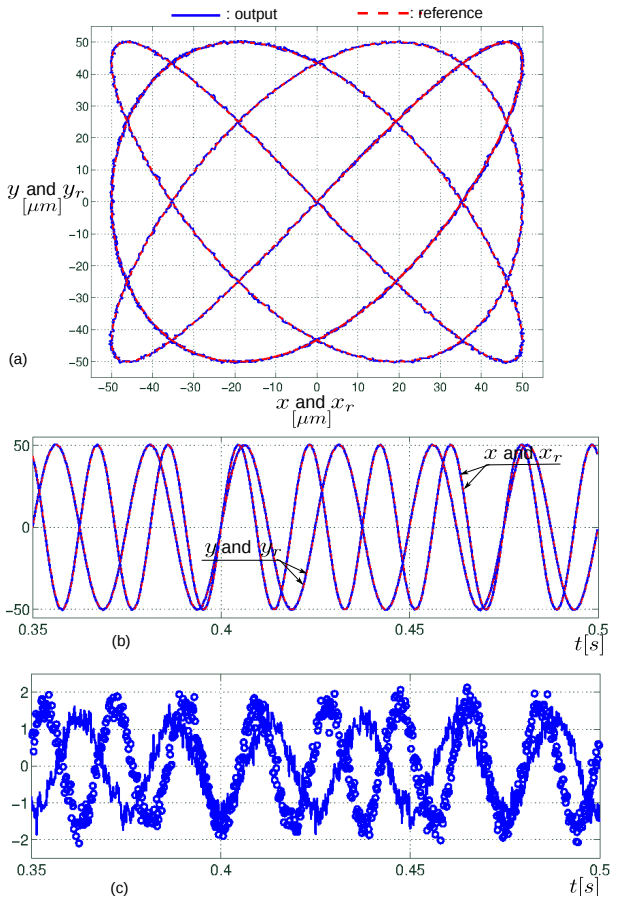

Fig 13: Tracking of Lissajous trajectory with a ratio of $r_f = \frac{4}{3}$.
(a): Lissajous curve, solid-line (—) is the Lissajous output whilst dashed-line (- -) is the Lissajous reference. (b): time domain tracking curves where solid-lines (—) are the outputs $x(t)$ and $y(t)$ and dashed-lines (- -) are the references $x_r(t)$ and $y_r(t)$. (c): tracking error.

6. REMARKS AND DISCUSSION

The approach suggested and developed in this paper is based on the classical Prandtl-Ishlinskii approach which is symmetrical and rate-independent (or static). Being rate-independent, the model and the compensator are valid at a single frequency, which is the identification frequency. However, the extensive experiments show that if the identification frequency f_k is in a domain where the phase-lag does not interfer, i.e. a frequency much lower than the bandwidth of the process, the model and the compensator are still valid for different excitation frequencies lower than f_k or slightly higher than this. Nevertheless, if the excitation frequency is too low, i.e. in a domain where the creep nonlinearity affects, the identified model and the compensator may not be anymore efficient. For applications that require working at such low frequency, a re-identification of the model and re-calculation of the compensator with lower f_k are required. Another way to tackle the modeling and compensation of hysteresis at different frequencies is to combine the proposed multivariable approach with a multivariable linear dynamics by cascading them. Such combination, called Hammerstein scheme, is usual in monovariable (SISO) case [6,7,40], and is a very interesting feature to be developed for the multivariable (MIMO) case. Finally, a last feature to tackle hysteresis at different frequencies consists in extending the monovariable rate-dependent Prandtl-Ishlinskii approach such as in [41] into multivariable.

The signals used during the characterization, identification and compensation in this paper were based on sine wave. In some applications, like atomic force microscopy, triangular waves are employed. In this case, to make the compensator efficient, it is recommended to also use triangular waves during the characterization and identification. In fact, triangular signals contain higher frequencies that a compensator calculated from a sine wave would not have been seen.

The compensator which was proposed in this paper utilizes a one-period delay, (see Theo. 4..1 and Fig. 3). A filter (for instance a 1^{st} order filter) with a conveniently chosen bandwidth can also be used in replacement of this delay-block. The bandwidth of the filter should be high enough to not modify the gain and phase of the compensator.

7. CONCLUSION

This paper deals with the modeling and the control of multivariable hysteresis in multi-dof systems and actuators. Based on the extension of the classical Prandtl-Ishlinskii (monovariable) model, the new multivariable model permits to account for the hysteresis in the direct transfers as well as the hysteresis in the cross-coupling transfers. Then a novel multivariable compensator is developed based on the restructuration of the multivariable model. An advantage of this restructuration is the inversion-free of the model itself and the extra-calculation of the compensator parameters avoided. This latter point is important since the number of parameters rapidly increases with the number of dof in the process. Finally, the developed multivariable modeling and compensation are applied to model a two-dof piezoactuator, to cancel its hysteresis and to reduce the cross-couplings. Extensive experiments with complex reference trajectories were carried out and demonstrated the efficiency of the approach.

ACKNOWLEDGMENT

This work was partially supported by the Labex-ACTION project (ANR-11-LABX-0001-01).

APPENDIX - PARAMETERS IDENTIFICATION FOR THE MONOVARIABLE CASE

Consider the classical Prandtl-Ishlinskii model in equ 2, which is monovariable. Following the procedure in [22], the identification of the thresholds parameters r_i and the weightings parameters w_i is performed by applying a sine input $u(t)$ with an amplitude u_A to the process. This amplitude corresponds to the maximal output of $y(t)$ that is expected for the applications. The curve in the $(u(t), y(t))$-map - which is a hysteresis - should be afterwards shifted so that it is in the positive section of the map before calculating the parameters. Fig. 14 shows an example of a (shifted) hysteresis curve approximated by three backlashes. In Fig. 14, $bw_i = 2 \cdot r_i$ are the bandwidth. From this figure, we write the j^{th} output:

$$y_j = \sum_{i=1}^{j} \left(bw_{j+1} - bw_i\right) \cdot w_i \tag{14}$$

From the previous equation, the following tensorial formulation is yielded:

$$\{y\} = [A] \cdot \{w\} \tag{15}$$

where $[A]$ is a triangular matrix constructed from the different bandwidths:

$$[A] = \begin{pmatrix} (bw_2 - bw_1) & 0 & \cdots & 0 \\ (bw_3 - bw_1) & (bw_3 - bw_2) & \ddots & \vdots \\ \vdots & \vdots & \ddots & 0 \\ (bw_{n+1} - bw_1) & (bw_{n+1} - bw_2) & \cdots & (bw_{n+1} - bw_n) \end{pmatrix} \tag{16}$$

The identification procedure is therefore as follows [22].

- Apply a sine input $u(t)$ to the actuator. The amplitude of the resulting output $y(t)$ should cover the end use range.
- If the obtained hysteresis curve is not in the positive section of the $(u(t), y(t))$-map, shift the curve.
- Define the number n of the backlashes.
- Split the input u domain into $n+1$ uniform or non-uniform partitions. For example, Fig. 14 depicts four partitions and presents an approximation of hysteresis with three backlashes. The bandwidth bw_i are calculated from the partition and the output vector $\{y\}$ is constructed from the ascending curve of Fig. 14.
- Construct the matrix $[A]$ from the bandwidth bw_i by using (equ 16),
- Finally, compute the parameter $\{w\}$ using the following formula:

$$\{w\} = [A]^{-1} \cdot \{y\} \tag{17}$$

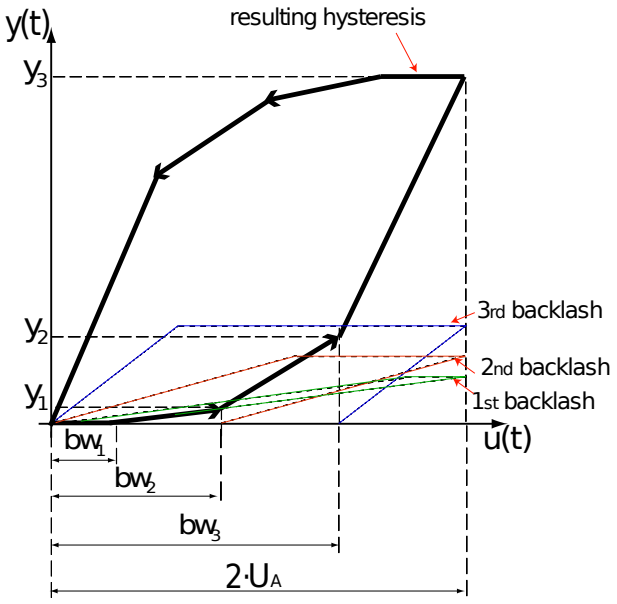

Fig 14: Example of (shifted) hysteresis constructed with three backlashes.

REFERENCES

[1] J. Agnus et *al*, 'Robotic Microassembly and micromanipulation at FEMTO-ST', Journal of Micro-Bio Robotics, vol.8(2), pages 91-106, 2013.

[2] S. Devasia, E. E. Eleftheriou, R. Moheimani, 'A survey of control issues in nanopositioning' IEEE Transactions on Control System Technology, Vol.15(15), pages 802-823, 2007.

[3] G. Binnig and H. Rohrer, 'Scanning tunneling microscopy', Helvetica Phys. Acta, vol.55, pp.726-735, 1982.

[4] M. Rakotondrabe and A. Ivan, 'Development and dynamic modeling of a new hybrid thermo-piezoelectric micro-actuator', IEEE Transactions on Robotics, Vol.26, Issue.6, pp.1077-1085, December 2010.

[5] G. Binnig, C. F. Quate, and C. Gerber, 'Atomic force microscope', Phys. Rev. Lett., vol.56(9), pp.930-933, March 1986.

[6] M. Rakotondrabe, C. Clévy and P. Lutz, 'Complete open loop control of hysteretic, creeped and oscillating piezoelectric cantilevers', IEEE Transactions on Automation Science and Engineering, Vol.7(3), pages 440-450, July 2009.

[7] D. Croft, G. Shed and S. Devasia, 'Creep, hysteresis and vibration compensation for piezoactuators: atomic force microscopy application', ASME Journal of Dynamic Systems, Measurement and Control, Vol.123(1), pages 35-43, March 2001.

[8] M. Rakotondrabe, 'Bouc-Wen modeling and inverse multiplicative structure to compensate hysteresis nonlinearity in piezoelectric actuators', IEEE Trans-

actions on Automation Science and Engineering, Vol.8(2), pages 428-431, April 2011.

[9] D. Habineza, M. Rakotondrabe and Y. Le Gorrec, 'Bouc-Wen Modeling and Feedforward Control of multivariable Hysteresis in Piezoelectric Systems: Application to a 3-DoF Piezotube scanner', IEEE Transactions on Control Systems Technology, DOI.10.1109/TCST.2014.2386779.

[10] S. Bashash and N. Jalili, 'A Polynomial-Based Linear Mapping Strategy for Feedforward Compensation of Hysteresis in Piezoelectric Actuators', ASME Journal of Dynamic Systems, Measurement and Control, Vol.130(3), 10 pages, DOI.10.1115/1.2907372, May 2008.

[11] K. Kyle Eddy, 'Actuator bias prediction using lookup-table hysteresis modeling', US Patent-08/846545, February 1999.

[12] A. Dubra and J. Massa and C.l Paterson, 'Preisach classical and nonlinear modeling of hysteresis in piezoceramic deformable mirrors', Optics Express, Vol.13(22), pages 9062-9070, 2005.

[13] X. Tan and J. S. Baras, 'Modeling and control of hysteresis in magnetostrictive actuators,' Automatica, vol.40(9), pages 1469-1480, 2004.

[14] D. H. Ji, J. H. Koo, W. J. Yoo, J. H. Park, 'Precise tracking control of piezoelectric actuators based on a hysteresis observer', Nonlinear Dynamics, 70(3), pp 1969-1976, 2012

[15] D. Hughes and J. T. Wen, 'Preisach modeling and compensation for smart material hysteresis,' Active Materials and Smart Structures, vol.2427, pages.50-64, 1994.

[16] L. Fang, J. Wang, Q. Zhang, 'Identification of extended Hammerstein systems with hysteresis-type input nonlinearities described by Preisach model', Nonlinear Dynamics, 79(2), 1257-1273, 2015.

[17] J. Manuel Cruz-Hernandez and V. Hayward, 'Phase Control Approach to Hysteresis Reduction', IEEE Transactions on Control Systems Technology, Vol.9(1), January 2001.

[18] W. T. Ang, P. K. Kholsa and C. N. Riviere, 'Feedforward controller with inverse rate-dependent model for piezoelectric actuators in trajectory-tracking applications', IEEE/ASME Transactions on Mechatronics, Vol.12(2), pages 134-142, April 2007.

[19] H. Jiang, H. Ji, J. Qiu and Y. Chen, 'A modified prandtl-ishlinskii model for modeling asymmetric hysteresis of piezoelectric actuators', IEEE Transactions on Ultrasonics, Ferroelectrics, and Frequency Control, Vol.57(5), pages 1200-1210, May 2008.

[20] K. Kuhnen and H. Janocha, 'Inverse feedforwrad controller for complex hysteretic nonlinearities in smart-materials systems', Control of Intelligent System, Vol.29(3), 2001.

[21] M. Al Janaideh, S. Rakheja, C. Y. Su, 'An analytical generalized Prandtl-Ishlinskii model inversion for hysteresis compensation in micropositioning control', IEEE/ASME on Transactions Mechatronics, Vol.16(4), 734-744

[22] M. Rakotondrabe, 'Classical Prandtl-Ishlinskii modeling and inverse multiplicative structure to compensate hysteresis in piezoactuators', American Control Conference, pages 1646-1651, Montréal Canada, June 2012.

[23] X. Liu, Y. Wang, J. Geng and Z. Chen, 'Modeling of hystersis in piezoelectric actuator based on adaptive filter', Sensors and Actuators A: Physical, vol.189, pp.420-428, 2013.

[24] U.X. Tan, W.T. Latt, F. Widjaja, C.Y. Shee, C.N. Riviere and W.T. Ang, 'Tracking Control of Hysteretic Piezoelectric Actuator using Adaptive Rate-Dependent Controller', Sensors and Actuators A: Physical, vol.150, pp.116-123, 2009.

[25] G-Y. Gu, L-M. Zhu and C-Y. Su, 'Modeling and Compensation of Asymmetric Hysteresis Nonlinearity for Piezoceramic Actuators With a Modified Prandtl-Ishlinskii Model', IEEE Transactions on Industrial Electronics, vol.61(3), pp.1583-1595, 2014.

[26] H. Shibly, D. Soffker, 'Mathematical models of shape memory alloy behavior for online and fast prediction of the hysteretic behavior', Nonlinear Dynamics, 62(1), 53-66, 2010.

[27] M. Basso, D. Materassi, M. Salapaka, 'Hysteresis models of dynamic mode atomic force microscopes: analysis and identification via harmonic balance', Nonlinear Dynamics, 54(4), 297-306, 2008.

[28] A. Bergander, W. Driesen, T. Varidel, M. Meizoso and J. M. Breguet, 'Mobile *cm*3-microrobots with tools for nanoscale imaging and micromanipulation', Mechatronics & Robotics, pages 1041-1047, Aachen Germany, September 2004.

[29] R. Perez, J. Agnus, C. Clévy, A. Hubert, N. Chaillet,'Modelling, fabrication and validation of a high performance 2 DOF piezoactuator for manipulation', IEEE/ASME Transactions on Mechatronics, Vol. 10(2), pages.161-171, 2005.

[30] I.D. Mayergoyz, 'Mathematical models of hysteresis', ISBN.0387973524, 3540973524, Springer-Verlag in New York, 1991.

[31] T. Matsuo and M. Shimasaki, 'Generalization of an isotropic vector hysteresis model represented by the superposition of stop models-Identification and rotational hysteresis loss,' IEEE Transactions on Magnetics, Vol.43, pages 1389-1392, April 2007.

[32] J. V. Leite, N. Sadowski, P. Kuo-Peng, and J. P. A. Bastos, 'A new anisotropic vector hysteresis model based on stop hysterons,' IEEE Transactions on Magnetics, vol.41, pages 1500-1503, May 2005.

[33] M. Kuczmann, 'Vector Preisach hysteresis modeling: Measurement, identification and application',

Elsevier Physica B: Condensed Matter, Vol.406(8), pages 1403-1409, 2011.

[34] M. Kuczmann, L. Stoleriu, 'Anisotropic Vector Preisach Model', Journal of Advanced Research in Physics, Vol.1(1), 011009, 2010.

[35] M. A. Krasnosel'skii and A. V. Pokrovskii, 'Systems with hysteresis', Springer-Verlag, Berlin, 1989.

[36] J. Agnus, P. De Lit and N.Chaillet, 'Micromanipulateur piézoélectrique notamment pour la microrobotique', french-patent, FR0211934, 2002.

[37] M. Rakotondrabe, 'Smart materials-based actuators at the micro/nano-scale: characterization, control and applications', edited book, Springer - Verlag, New York, ISBN 978-1-4614-6683-3, 2013.

[38] M. Rakotondrabe, 'Modeling and Compensation of Multivariable Creep in multi-DOF Piezoelectric Actuators', IEEE Intern Conf on Robotics and Automation, pp.4577-4581, St Paul Minnesota USA, May 2012.

[39] T. Tuma, J. Lygeros, A. Sebastian and A. Pantazi, 'Optimal scan trajectories for high-speed scanning probe microscopy', American Control Conference, pages 3791-3796, MontrÃl'al Canada, June 2012.

[40] M. Al Janaideh and M. Rakotondrabe, 'Further Results on Hysteresis Compensation of Smart Micro-Positioning Systems with the Inverse Prandtl-Ishlinskii Compensator, IEEE Transactions on Control Systems Technology, doi:10.1109/TCST.2015.2446959.

[41] O. Aljanaideh, M. Al Janaideh and M. Rakotondrabe, 'Enhancement of Micro-positioning Accuracy of a Piezoelectric Positioner by Suppressing the Rate-Dependant Hysteresis Nonlinearities', IEEE/ASME Intern Conf on Advanced Intelligent Mechatronics, pp.1683-1688, Besancon, France, July 2014